FIRST PRINCIPLE COMPUTATIONAL STUDIES ON THE ELECTRONIC STRUCTURE OF MUONATED κ-(BEDT-TTF)$_2$Cu[N(CN)$_2$]Cl and κ-d8-(BEDT-TTF)$_2$Cu[N(CN)$_2$]Br

DANG FATIHAH BINTI HASAN BASERI

UNIVERSITI SAINS MALAYSIA

2022

FIRST PRINCIPLE COMPUTATIONAL STUDIES ON THE ELECTRONIC STRUCTURE OF MUONATED κ-(BEDT-TTF)$_2$Cu[N(CN)$_2$]Cl and κ-d8-(BEDT-TTF)$_2$Cu[N(CN)$_2$]Br

by

DANG FATIHAH BT HASAN BASERI

Thesis submitted in fulfillment of the requirements
for the Degree of
Doctor of Philosophy

January 2022

ACKNOWLEDGEMENT

First and foremost, I would like to express my gratitude to Almighty Allah for HIS graces and blessings. I also would like to express my heartiest gratitude to my research supervisor, Prof. Dr. Shukri Sulaiman as well as my co-supervisor Assoc. Prof. Dr. Mohamed Ismail Mohamed Ibrahim for providing invaluable guidance, comments and suggestions throughout my study. I am extremely grateful to my husband, parents and family for their support, prayers and sacrifices along my PhD journey. I am particularly indebted to them for their unceasing encouragements and supports. Also, I express my thanks to my laboratory colleagues for their sincere and encouraging guidance and elevating inspiration and also thanks for the great work environment. It is also my honour to convey my thankfulness to the Ministry of Higher Education for providing me “the MyBrain scholarship” for this study. In addition, I also take this opportunity to acknowledge HOKUSAI Greatwave Supercomputer in Japan for providing great access to the powerful supercomputer. Finally, gratitude goes to everyone who contributed directly or indirectly to this project.

TABLE OF CONTENTS

ACKNOWLEDGEMENT ..... **ii**
TABLE OF CONTENTS ..... **iii**
LIST OF TABLES ..... **viii**
LIST OF FIGURES ..... **ix**
LIST OF ABBREVIATIONS ..... **xii**
LIST OF APPENDICES ..... **xiiv**
ABSTRACT ..... **xvii**
CHAPTER 1 INTRODUCTION **1**
1.1 Research Background 1
1.1.1 Problem Statements 5
1.1.2 Objectives 6
1.1.3 Scope of Study 6
1.1.4 Research Motivation 8
1.2 Chapter Summary 8
CHAPTER 2 LITERATURE REVIEW **9**
2.1 Organic Magnet 9
2.2 Mott Insulator 11
2.3 BEDT-TTF Molecule 12
2.4 $(BEDT\text{-}TTF)_2X$ Compound 14
2.5 κ-$(BEDT\text{-}TTF)_2Cu[N(CN)_2]Cl$ 19
2.6 κ-d8-$(BEDT\text{-}TTF)_2Cu[N(CN)_2]Br$ 25
2.7 Muon and Muonium 28
2.8 Chapter Summary 31
CHAPTER 3 METHODOLOGY **32**
3.1 Computational Methods 32
3.1.1 Electronic Structure Methods 33
3.1.2 Density Functional Theory 35
3.1.3 Hartree-Fock (HF) 37
3.2 Molecular Orbital Theory 37
3.3 Theoretical Overview 39

3.3.1 The Schrodinger Equation 39
3.3.2 The Born-Oppenheimer 41
3.4 Software 42
3.4.1 Gaussian16 42
3.4.2 Gauss View 5.0 43
3.4.3 Natural Bond Orbital (NBO) 44
3.4.4 AOMix 6.86 44
3.4.5 Amsterdam Density Functional (ADF) 44
3.5 Basis Set 45
3.6 Pure System of κ-(BEDT-TTF)2Cu[N(CN)2]Cl and κ-d8-(BEDT-TTF)2Cu[N(CN)2]Br. 49
3.7 Muonated κ-(BEDT-TTF)$_2$Cu[N(CN)$_2$]Cl and κ-d8-(BEDT-TTF)2Cu[N(CN)2]Br 50
3.8 Theoretical computation 51
3.8.1 Generating Input Files 51
3.8.2 Single Point Energy Calculations 52
3.8.3 Geometry Optimization 53
3.8.4 Effective exchange coupling constant (J_{ij}) 54
3.8.5 Broken-symmetry approach 54
3.8.6 Hyperfine interaction 55
3.8.7 Vibrational averaging 56
3.9 Chapter Summary 57
CHAPTER 4 RESULTS AND DISCUSSION 58
4.1 Introductions 58
4.2 ET molecule 61
4.3 Pure system of κ-(BEDT-TTF)$_2$Cu[N(CN)$_2$]Cl 63
4.3.1 Electronic structures of one fragment cluster 63
4.3.1(a) Spin density 63
4.3.1(b) Frontier Molecular Orbital Analysis 65
4.3.1(c) Atomic charges 68
4.3.2 Electronic structures of two fragments κ-Cl 71
4.3.2(a) Spin density 71
4.3.3 Calculations of exchange coupling constants (J_{ij}) of κ-Cl 73

4.3.4 Electronic structures of three fragments κ-Cl 75
4.3.4(a) Total energy 75
4.3.4(b) Spin density 76
4.3.5 Possible magnetic structures of κ-Cl 78
4.4 Muonated system of κ-(BEDT-TTF)$_2$Cu[N(CN)$_2$]Cl 80
4.4.1 Geometrical structures 80
4.4.2 Electronic structures 82
4.4.2(a) Total energy 82
4.4.2(b) Spin density 83
3.4.2(c) Bond order 84
4.4.3 Hyperfine interactions 85
4.4.3(a) Vibrational averaging 87
4.5 Pure system of κ-d8-(BEDT-TTF)$_2$Cu[N(CN)$_2$]Br 91
4.5.1 Electronic structures of one fragment κ-d8-Br 91
4.5.1(a) Spin density 91
4.5.1(b) Frontier molecular orbital analysis 93
4.5.1(c) Atomic charges 95
4.5.2 Electronic structures of two fragments κ-d8-Br 98
4.5.2(a) Spin density 98
4.5.3 Calculations of exchange coupling constants (J_{ij}) of κ-d8-Br 100
4.5.4 Electronic structures of three fragments κ-d8-Br 101
4.5.4(a) Total energy 101
4.5.4(b) Spin density 102
4.5.5 Possible magnetic structures of κ-d8-Br 104
4.6 Muonated system of κ-d8-(BEDT-TTFR)$_2$Cu[N(CN)$_2$]Br 106
4.6.1 Geometrical structure 106
4.6.2 Electronic structure 107
4.6.2(a) Relative energy 107
4.6.2(b) Spin density 108
4.6.3 Hyperfine interaction 109
4.6.3(a) Vibrational Averaging 110
4.7 Chapter Summary 114
CHAPTER 5 115

CONCLUSION..... 115
5.1 Future Study 116
REFERENCES..... 117
APPENDICES

LIST OF TABLES

Page

Table 2.1 Properties of muonium and hydrogen 30
Table 4.1 Geometrical parameters of neutral ET before and after optimization . 62
Table 4.2 Composition of Alpha-spin molecular orbitals (%) 67
Table 4.3 Mulliken and Natural charges for the anion part 69
Table 4.4 Mulliken and Natural charges for cation part 69
Table 4.5 Values of exchange coupling interactions, J_{ij} for J_{12}, J_{23}, and J_{31} in meV unit 73
Table 4.6 Total energy of κ-Cl for AFM state and high spin state for M_{12}, M_{23}, and M_{31} 75
Table 4.7 Relative energy between high spin state and AFM state for M_{12}, M_{23}, and M_{31} (with respect to high spin state) 75
Table 4.8 Spin density of each fragment for three AFM configurations 76
Table 4.9 Geometrical parameters of optimized muonated κ-Cl 81
Table 4.10 Relative energy of muonated κ-Cl with respect to S1 position using Gaussian16 and ADF software 82
Table 4.11 Values of bond order for each muon sites 85
Table 4.12 Values of the hyperfine coupling constant (Gauss) for S1, S3, C9 and C7 87
Table 4.13 Values of the hyperfine coupling constants for C7, C9, S1 and S3 before and after vibrational averaging in Gauss unit 90
Table 4.14 Values of hfcc (Gauss) by μSR experiment and DFT calculations 90
Table 4.15 Composition of Alpha-spin molecular orbitals (%) for κ-d8-Br 94
Table 4.16 Mulliken and Natural charges for anion part 96
Table 4.17 Mulliken and Natural charges for cation part 97
Table 4.18 Values of exchange coupling interactions, J_{ij} for J_{12}, J_{23} and J_{32} 101
Table 4.19 Total energy of κ-d8-Br for AFM state and high spin state 102
Table 4.20 Relative energy (with respect to high spin state) 102

Table 4.21 Spin density for three AFM configurations 102
Table 4.22 Geometrical parameters of optimized muonated κ-d8-Br..... 107
Table 4.23 Relative energy of muonated κ-d8-Br with respect to the C5 position108
Table 4.24 Values of the hyperfine coupling constant (Gauss) for C5, C20, S14 and S17 110
Table 4.25 Values of the hyperfine coupling constant for S14, S17, C5 and C20 before and after vibrational averaging using ADF software..... 113
Table 4.26 Values of hfcc (Gauss) by μSR experiment and DFT calculations 113

LIST OF FIGURES

Page

Figure 2.1 Crystal structure of κ-ET from *c*-axis direction 16

Figure 2.2 The spin interactions between muon and electron 29

Figure 3.1 The illustration of the molecular orbital diagram of a hydrogen molecule 38

Figure 3.2 The numbering of atoms of κ-(BEDT-TTF)$_2$Cu[N(CN)$_2$]Cl 49

Figure 3.3 The numbering of atoms of κ-d8-(BEDT-TTF)$_2$Cu[N(CN)$_2$]Br 50

Figure 4.1 Structure of ET compound 60

Figure 4.2 Structure of κ-(BEDTTF)$_2$Cu[N(CN)$_2$]Cl 60

Figure 4.3 Structure of κ-d8-(BEDTTF)$_2$Cu[N(CN)$_2$]Br 61

Figure 4.4 Total spin densities for anion and cation 64

Figure 4.5 Percentage distributions of spin densities for S inner, S outer, C = and C – 64

Figure 4.6 HOMO-LUMO plot of κ-Cl 66

Figure 4.7 Total Mulliken charges for anion and cation 70

Figure 4.8 Spin distribution of the two fragments for AFM state. The blue and green colour represents α-spin and β-spin, respectively 72

Figure 4.9 Diagram of exchange coupling interactions, $\boldsymbol{J_{ij}}$ for: (a) High spin configurations. Circles and arrow respectively denote the dimers and spins. (b) Low spin configuration. The frustrated bonds are denoted by thick red lines. 73

Figure 4.10 Length of M_{12}, M_{23}, and M_{31} 73

Figure 4.11 Spin distributions of the three fragments for the AFM state. The blue and green colour represents α-spin and β-spin, respectively 77

Figure 4.12 Possible magnetic structure for κ-Cl. The red arrows indicate the spin up direction and the violet arrows indicate the spin down direction .. 78

Figure 4.13 Initial geometries of muonated κ-Cl 80

Figure 4.14 The distributions of Mulliken spin densities from (a) to (d) for S1, S3, C7 and C9 sites, respectively 83

Figure 4.15 Relative energy and Fermi contact for the vibration of C7 (a), C9 (b), S1 (c), and S3 (d) positions 89

Figure 4.16 Total spin densities for anion and cation 92
Figure 4.17 Percentage distributions of spin densities for S inner, S outer, C = and C– 93
Figure 4.18 HOMO LUMO energy diagram for κ-d8-Br 95
Figure 4.19 Total Mulliken charges for anion and cation 96
Figure 4.20 Spin distribution of the two fragments for the AFM state. The blue and green colour represents α-spin and β-spin, respectively 99
Figure 4.21 Length of M_{12}, M_{31} *and* M_{23} 100
Figure 4.22 Spin distribution of the three fragments for the AFM state. The blue and green colour represents α-spin and β-spin, respectively 104
Figure 4.23 Possible magnetic structure of κ-d8-Br. The red arrows indicate the spin up direction and the violet arrows indicate the spin down direction. 104
Figure 4.24 Initial geometries of muonated κ-d8-Br 106
Figure 4.25 The distributions of Mulliken spin densities from (a) to (d) for C5, C20, S14 and S17 sites, respectively 109
Figure 4.26 Relative energy and Fermi contact for the vibration of S14, S17, C5 and C20, positions 112

LIST OF ABBREVIATIONS

μSR	Muon spin rotation/relaxation/resonance
a.u	Atomic unit
ADF	Amsterdam Density Functional
AFM	Antiferromagnetic
AFMR	Antiferromagnetic resonance
AM1	Austin Model 1
B3LYP	Becke-3-Lee-Yang-Parr correlation functional
BEDT-TTF	Bis(ethylenedithio)tetrathiafulvalene
BNOO	Double perovskite Ba_2NaOsO_6
BSSE	Basis set superposition error
CCDC	Cambridge Crystallographic Data Centre
DFT	Density functional theory
DM	Dzyaloshinsky-Moriya
FM	Ferromagnetic
G16	Gaussian16
GTO	Gaussian type orbitals
hfcc	Hyperfine coupling constants
HOMO	Highest Occupied Molecular Orbital
KS	Kohn – Sham approach
LCAO-MO	Linear combination atomic orbitals, molecular orbitals
LUMO	Lowest Unoccupied Molecular Orbital
$M(dmit)_2$	Metal dithiolene complexes
MINDO/3	Modified Intermediate Neglect of Differential Overlap, version 3
MO	Molecular orbital
MPA	Mulliken Population Analysis
Mu	Muonium
NAOs	Natural atomic orbitals
NBO	Natural Bond Orbital
NMR	Nuclear magnetic resonance
NPA	Natural population analysis
O3LYP	Cohen-Handy-3-Lee-Yang-Parr correlation functional

PES	Potential energy surface
PM	Paramagnetic metal
PM3	Parametric Model number 3
SOC	Spin-orbit coupling
STM	Scanning tunnelling spectroscopy
STO	Slater type orbitals
STO-3G	Slater type orbitals simulated by 3 Gaussians added together
TCNE	Tetracyanoethylene
TMTSF	Tetramethyltetraselenafulvalene
TTF-TCNQ	Tetrathiafulvalene tetracyanoquinodimethane
TZVP	Valence triple-zeta polarization
UDFT	Unrestricted Density Functional Theory
UHF	Unrestricted Hartree-Fock
κ-ET	Bis (ethylenedithio)tetrathiafulvalene, $C_{10}H_8S_8$

LIST OF APPENDICES

APPENDIX A HYPERFINE INTERACTION

KAJIAN PERKOMPUTERAN PRINSIP PERTAMA ATAS STRUKTUR ELEKTRONIK PADA κ-(BEDT-TTF)$_2$Cu[N(CN)$_2$]Cl DAN κ-d8-(BEDT-TTF)$_2$Cu[N(CN)$_2$]Br TERMUONIASI

ABSTRAK

κ-(BEDT-TTF)$_2$Cu[N(CN)$_2$]Cl dan κ-d8-(BEDT-TTF)$_2$Cu[N(CN)$_2$]Br adalah bahan magnet organik dengan potensi aplikasi dalam 'spintronics'. Sejumlah data μSR pada struktur ini telah meningkat dengan cepat dan berterusan muncul dari masa ke semasa. Elektron yang tidak berpasangan biasanya berada di seluruh dimer dan tidak berada di sekitar atom tertentu yang boleh mempengaruhi sifat-sifat magnet sistem. Secara dasarnya, susunan jarak jauh momen magnet yang mengkonfigurasi struktur magnet sistem masih tidak jelas dan penyelidikan lebih lanjut diperlukan. Untuk melengkapkan kajian μSR, kaedah pengiraan Teori Fungsi Ketumpatan (DFT) telah dijalankan untuk menyiasat struktur elektronik dalam keadaan putaran tinggi dan keadaan antiferromagnetik (AFM) serta untuk memerhatikan jenis kemagnetan yang terdapat dalam sebatian ini. Oleh kerana jumlah tenaga yang diperoleh dalam keadaan AFM untuk konfigurasi M_{12}, M_{23}, and M_{31} adalah sedikit lebih stabil dibandingkan dengan tenaga untuk keadaan putaran tinggi, secara pengiraan terbukti bahawa keadaan dasar mempunyai konfigurasi AFM yang setara dengan hasil eksperimen. Tenaga relatif untuk M_{12} dalam keadaan AFM adalah paling rendah dengan nilai -0.016 eV untuk κ-(BEDT-TTF)$_2$Cu[N(CN)$_2$]Cl dan -0.015 eV untuk κ-d8-(BEDT-TTF)$_2$Cu[N(CN)$_2$]Br. Seperti yang dapat dilihat dari pengiraan sistem tulen, kepadatan putaran tidak bertempat pada atom tertentu tetapi bertebaran ke seluruh kation. Nilai kepadatan putaran pada anion dan kation adalah masing-masing 0.007 dan 0.993 untuk κ-(BEDT-TTF)$_2$Cu[N(CN)$_2$]Cl manakala untuk κ-d8-(BEDT-

$TTF)_2Cu[N(CN)_2]Br$ adalah masing-masing 0.005 dan 0.995 untuk anion dan kation. Selain itu, perhitungan pada sistem termuoniasi juga dilakukan untuk menentukan struktur elektronik dan juga tempat muon berhenti. Terdapat empat tapak penghentian muon yang dikira dalam kajian ini, iaitu di ikatan sulfur dalaman, sulfur luar dan dua ikatan pada dua karbon. Telah didapati bahawa muon lebih cenderung untuk berhenti di atom sulfur. Dua penjelasan yang mungkin dalam situasi ini ialah jumlah tenaga sebatian adalah lebih stabil di tapak sulfur dan nilai hfcc lebih setanding dengan eksperimen. Perbezaan peratus nilai hfcc antara eksperimen dan pengiraan pada sulfur adalah 39.2% dan 45.1% untuk κ-$(BEDT\text{-}TTF)_2Cu[N(CN)_2]Cl$ dan 24.3% dan 2.7% untuk κ-d8-$(BEDT\text{-}TTF)_2Cu[N(CN)_2]Br$. Pengiraan purata getaran akhirnya dilakukan untuk lima titik getaran untuk mengesahkan ketepatan hfcc. Nilai hfcc yang diperoleh selepas purata getaran sedikit berbeza, dengan perbezaan peratusan terletak antara julat 2.7% hingga 45.1%.

FIRST PRINCIPLE COMPUTATIONAL STUDIES ON THE ELECTRONIC STRUCTURE OF MUONATED κ-(BEDT-TTF)$_2$Cu[N(CN)$_2$]Cl and κ-d8-(BEDT-TTF)$_2$Cu[N(CN)$_2$]Br

ABSTRACT

κ-(BEDT-TTF)$_2$Cu[N(CN)$_2$]Cl and κ-d8-(BEDT-TTF)$_2$Cu[N(CN)$_2$]Br are organic magnet materials with potential application in spintronics. The number of μSR data on this structure has increased rapidly and continuously appear from time to time. An unpaired electron is generally localized throughout the dimer and is not localized around a particular atom which can affect the magnetic properties of the system. Intrinsically, the long-range ordering of the magnetic moments that was configured by the magnetic structure of the system remains unclear and further investigations are required. In order to complement the μSR study, the Density Functional Theory (DFT) computational method has been performed to investigate the electronic structures in the high spin and antiferromagnetic (AFM) state as well as to observe the type of the magnetism that exists in this compound. As the total energy obtained in an AFM state for M_{12}, M_{23}, and M_{31} configurations are slightly more stable compared to the high spin state, it is computationally proved that the ground state possessed an AFM configuration. The relative energy for M_{12} in the AFM state are discovered to have the lowest energy with the value of -0.016 eV for κ-(BEDT-TTF)$_2$Cu[N(CN)$_2$]Cl and -0.015 eV for κ-d8-(BEDT-TTF)$_2$Cu[N(CN)$_2$]Br. This result is essentially equivalent to the experimental result. As shown from the calculations of the pure system, the spin densities are not localized on any particular atom but distributed throughout the cation. The values of spin densities at the anion and cation sites are 0.007 and 0.993 respectively for κ-

(BEDT-TTF)$_2$Cu[N(CN)$_2$]Cl while for κ-d8-(BEDT-TTF)$_2$Cu[N(CN)$_2$]Br are 0.005 and 0.995 for anion and cation sites respectively. The calculations on the muonated system were also performed to determine the electronic structures as well as the muon stopping sites. There are four muon stopping sites calculated in this study. The sites are at the inner sulphur, outer sulphur and two carbon double bonds. It has been found that the muon is more feasible to stop at sulphur atoms. Two possible explanations for this situation are the fact that the total energies of the compounds are more stable at sulphur sites and that the hfcc values are more comparable to experiment. The percentage difference of hfcc between experimental values and calculated values at sulphur sites are 39.2% and 45.1% for κ-(BEDT-TTF)$_2$Cu[N(CN)$_2$]Cl and 24.3% and 2.7% for κ-d8-(BEDT-TTF)$_2$Cu[N(CN)$_2$]Br. Vibrational averaging calculations were eventually performed for five points of vibrations to confirm accuracy of the hfcc. The hfcc values obtained after vibrational averaging are slightly different, with the percentage of differences ranging between 2.7% to 45.1%.

Chapter 1

INTRODUCTION

1.1 Research Background

Magnetism in organic compounds has great potential in electronic industry. The strength of the magnetic field produced by organic compounds is very small as compared to the conventional magnets. However, it could be sufficient for application such as spintronic. The long range magnetic ordering in most of these organic compounds is antiferromagnetic (AFM) [1]–[4]. There are a few organic compound series such as TMTSF (tetramethyltetraselenafulvalene), TTF-TCNQ (tetrathiafulvalene tetracyanoquinodimethane), BEDT-TTF (bis (ethylenedithio)tetrathiafulvalene) and $M(dmit)_2$ (metal dithiolene complexes) salts which gathered much attention among researchers. The TTF-TCNQ and TMTSF exhibit a unique low-dimensional (1-D) crystal structure [5]–[7] while BEDT-TTF and $M(dmit)_2$ show 2-D crystal structure [8], [9]. Some of the compounds in the BEDT-TTF series such as the κ-phase salts of BEDT-TTF are particularly very interesting, because aside from exhibiting a long range magnetic ordering, they are also Mott insulators and can make a transition to superconducting state [10]–[12] .

Of particular interest are the organic charge-transfer κ-phase salts, κ-$(BEDT\text{-}TTF)_2Cu[N(CN)_2]X$. These compounds contain a cation and an anion, $(BEDT\text{-}TTF)_2^+$ and $Cu[N(CN)_2]X^-$ respectively. ($Cu[N(CN)_2]X \equiv$ copper dicyanamide halide). X is a halogen, either Cl, Br, or I. These series are also abbreviated as κ-ET. The notation κ refers to their crystal structure which is orthorhombic. The properties

of these series are tunable by changing X, temperature and pressure. They can either become a ferromagnet (FM), AFM, superconductor, Mott insulator or metal.

Apart from the application in spintronic as mentioned above, κ-ET also possesses other important properties such as spin liquid phases which depend on the temperature, pressure and the anion part [13]. In terms of superconductivity, κ-Br exhibits superconducting state at ambient pressure with T_c = 11.6 K [14] while κ-I did not show the superconducting state under any conditions [15]. On the other hand, κ-Cl is a paramagnetic insulator [2]. It exhibits superconducting properties at an applied pressure of 0.3 kbar with T_c = 11.5 K [16]. κ-Cl is well-known to have the highest T_c among its derivatives [15] .

This research focuses on bis(ethylenedithio)tetrathiafulvalene, κ-ET salts with copper dicyanamide chloride and bromide anions abbreviated as κ-Cl and κ-d8-Br respectively, as they exhibit AFM configurations on the ground state [17], [18] . Both organic compounds possess some general characteristics, which they can be treated as two-dimensional systems and their physical properties are determined by the overlap of the molecular orbitals (MO) [19]. Both materials also share similar delocalized behavior of the unpaired electron, which the delocalization presented throughout the cation part. Numerous investigations are continuously performed over the past few years to study κ-Cl and κ-d8-Br compound experimentally, such as muon spin rotation/relaxation/resonance (μSR) techniques [20], magnetization measurement [17, 18], thermal expansion measurement [23], ESR spectroscopy [24], Raman scattering spectra [25] and so forth. Although there are huge numbers of experiments in the literature, detailed computational studies performed on this structure remain rare. From the best of our knowledge, the experimental study can

investigate many properties of the system, but the limitations still exist. This limitation, however, can be overcome by the theoretical studies, which is also very valuable to aid the interpretation of experimental data.

The μSR spectroscopic technique is known to be more related to this study since both experimental and theoretical has using a positive muon as a local probe to investigate the properties of the target systems. In theoretical calculations, hydrogen which resembles muonium (Mu) will attach to the system and corrected for the difference in the gyromagnetic ratios of H and Mu. Mu is a light isotope of hydrogen and exhibits the same chemical behavior. The Bohr radius and ionization energy are about 0.5% of hydrogen, deuterium, and tritium [26]. Therefore, hydrogen is the perfect atom to represent Mu as the Mu properties similar to that of hydrogen. As muon is sensitive probes of magnetic and electronic quantum [26], it can be the most powerful medium to investigate the materials both experimentally and theoretically. Possible muon site has become the center of interest for both types of study. The muon stopping sites in a sample have been recognized to be crucial since associated muon hyperfine interactions provide information about the local fields owing to the electron spins distribution in the system. Muonium hyperfine interaction is proved to be sensitive to the local electron spin distribution [27]. It can effectively examine the local environment in the vicinity of Mu position. μSR experiment can obtain the hyperfine interactions at the muon site. The information on the muon stopping sites, however, is unable to determine experimentally. Therefore, computational studies are crucial to assist in the interpretation and analysis of the μSR data. It can provide a general idea of the possible location of the muon. Once the site of the muon is confirmed, the hyperfine interactions examine by the theoretical study will be compared with the hyperfine field obtained by the stringent μSR experimental tests.

At this stage, the accuracy of the electronic structure obtained by theoretical calculation can be verified. The data on the electronic structure is inferred to be correct if the hyperfine interactions obtained from both studies are in a good agreement. This is the most apparent reason why the location of the muon is very crucial for this study. Hence, further microscopic properties such as spin and charge distributions, nature of bonding, molecular orbitals, magnetically ordered states and other intriguing properties can be determined, which are unable to obtain through the μSR experiments. Such accurate electronic structures calculated are of great importance in determining the origin of magnetism for the target systems. On the other hand, the computational studies on the electronic structures also act as a crucial ingredient for a deeper understanding on the dynamics of electrons as observed through the μSR experiments.

The μSR technique is powerful in characterizing free radicals in all three phases including solid, liquid or gaseous. μSR is referring to three different techniques applied; muon spin rotation, relaxation and resonance. This technique is very sensitive to detect the presence of small magnetic field as well as small magnetic moments [28]. Its sensitivity renders this technique to be extremely useful in determining various magnetic and superconducting materials such as pyrochlore antiferromagnets [29], ferrimagnetic molecular magnet [30] and organic superconductors [31]. Recently, a μSR experimental study was conducted to investigate the possible muon sites on κ-Cl with experimental and calculated the values of the internal field [20].

Throughout this research, MO cluster method was applied. MO cluster method is a method which considers a small group of atoms as a region of interest to

represent an infinite system. This method is applied due to the fact that it is not computationally feasible to take an infinite system to perform a calculation.

1.1.1 Problem Statements

A number of μSR experimental data on the κ-Cl and κ-d8-Br have been reported in the literature. Recent studies on κ-Cl have reported on the muon hyperfine field [20]. In another piece of literature, muon-electron hfcc are determined for κ-d8-Br [32]. However, there are lacks of detailed computational studies on these structures. This is lies in the difficulties to calculate the organic molecules with a large size and complex crystal structures.

The most important aspect related to the μSR experiments is the information of the muon stopping sites in the studied materials. It should be noted that in an experiment, the limitations in collecting the data still exist as they cannot provide information on the position of Mu owing to insufficient experimental information. In addition, the magnetic structures of these systems are experimentally unknown. Therefore, the computational studies can be very valuable to understand the underlying physics behind the observer properties as well as to obtain an idea about the position of muon. The magnetism of these materials also remains unclear, particularly the magnetic structure of the systems. Hence, the long-range magnetic ordering can be revealed through computational study.

1.1.2 Objectives

Three ultimate objectives in conducting this research are listed as below:

1. To analyze the electronic structures of κ-Cl and κ-d8-Br.
2. To investigate the AFM configuration as the ground state of κ-Cl and κ-d8-Br.
3. To study muon stopping sites and its associated hyperfine coupling constant (hfcc) in the systems.

1.1.3 Scope of Study

In this research, two compounds of κ-ET family; κ-Cl and κ-d8-Br were studied as both materials exhibit AFM ordering. Calculations for the two compounds were performed for pure and muonated systems. A full picture of the electronic structures of the pure and muonated systems is crucial to understand the underlying physics behind the unique characteristics of each material.

Conceptually, it is insufficient to utilize only one type of software to perform calculations. This claim is supported on the fact that each of the software has their own specific functions. Therefore, there are three different sotware employed in these studies. One of the software utilized in these calculations is Gaussian16 (G16) software [33]. Apart from that, Gauss View 5 software [34] was also been used as a graphical interface. In this study, G16 software was focused on obtaining the simple electronic structures such as the total energy of the molecules, HOMO-LUMO energy, electron spin density, natural population analysis (NPA) and magnetic structures of the systems. On the other hand, ADF software was utilized to calculate

the muon hyperfine coupling constants (hfcc) owing to the fact that it is well-known to produce good results on hfcc [35]. The ultimate goal of this research is to determine the hfcc as clearly stated in the objectives above. The hfcc values obtained from the calculations can be very valuable to obtain a general idea about the muon stopping site. μSR experiment can obtain the hyperfine interactions at the muon site but has a limitation in determining the muon stopping site. The determination of possible muon site is essential to test the accuracy of the electronic structure of the studied system. This is the most apparent reason on why the determining of hfcc is very crucial. The calculated hfcc values were then will compare with the value of muon internal field obtained from μSR experiment to identify whether hfcc values from calculations are in a good agreement with the one from the experiment.

The geometries were optimized using Hartree-Fock level utilizing small-size STO-3G basis set while the single point energy calculation was evaluated at the DFT method coupled with 6-311++G** basis sets. Higher basis set was utilized to obtain accurate results on the electronic structures. Diffuse functions are essential to be added as both compounds contain the anion part.

Due to limited computing resources at Hokusai GreatWave Supercomputing Facility, RIKEN Advanced Center for Computing and Communication, all calculations were performed using three fragments of molecules only. Calculation including more than three fragments is not feasible because it requires more computing resources than what have been allocated for this study.

1.1.4 Research Motivation

In recent years, there has been an increasing interest in organic charge transfer salts, BEDT-TTF, such as κ-Cl and κ-d8-Br. However, the magnetic structures of these systems with the ground state are still not fully determined. Further studies need to be undertaken to understand the underlying electronic structure that influences the long-range magnetic ordering. An accurate determination of the electronic structures is crucial in determining the origin of magnetism for the target systems. However, there is an apparent lack of computational work to confirm the magnetic structure. Therefore, the motivation of this study is to investigate the electronic and magnetic structure of κ-Cl and κ-d8-Br using the novel DFT methodology.

1.2 Chapter Summary

Research background in Chapter 1 comprises four subtopics: problem statements, objectives, scope of study, and research motivation. The research background included a brief explanation of organics magnet and focused more on the κ-ET salts. On the other hand, problem statements, objectives, and scope of study, including the limitation of this study and its motivation, were stated clearly in respective subtopics.

Chapter 2

Literature Review

2.1 Organic Magnet

Organic magnet can be define as an organic material which showing bulk magnetic ordering which contributed by an unpaired electron spins occupy in *p*-orbital [36]. This is inconsistent with the conventional magnetic materials which possess unpaired electron spins in *d*- or *f*- orbitals. Unpaired electron spins are responsible to form magnetic materials. It is very well-known that the electronic properties of a system are characterized by its electron whereas electrical properties are described by the electron dynamics of the materials. Magnetism is also shown to be related to the electron.

Pauli Exclusion Principle states that each orbital can consist of two electrons which one is spin up and the other one is spin down and the total magnetic moment is zero. In addition, the electrons required to occupy spin up positions in the same orbital energy. The magnetic moments are formed by these spin-up electrons. Spins which designated by an arrow can couple in a few different alignments. Such for FM coupling, the spin will couple in the same directions. When the spins oppose each other, it is known to be an AFM. The spins for AFM ordering are identical and will be cancelling each other resulting in zero net moments.

Generally, magnetism can be classified into two types; induced and spontaneous magnetism. The former type of magnetism arises with the presence of the external magnetic fields. It can be either diamagnetic or paramagnetic. Materials with diamagnetic magnetism have no permanent net atomic magnetic moment since the orientations of electrons cancel each other. All organic materials formally exhibit

this kind of magnetism. Paramagnetic occurs with the presence of unpaired electrons as long as the realignment of the path of the electrons affected by the external magnetic field. The spins do not interact with other spins and their orientations are ransom and fluctuate with time. The magnetic properties for both diamagnetic and paramagnetic materials will disappear once the external field is removed. For spontaneous magnetism, the magnetic properties appear in the absence of a magnetic field. The presence of the magnetic moment of an atom in the absence of a magnetic field is based on two factors which are the orbital angular momentum of the electrons and the spin itself. The combinations of these two factors will contribute to the permanent magnetic moment. Ferromagnetic and ferrimagnetic materials are a part of magnetism which categorized in the spontaneous type of magnetism. Ferrimagnets occur from AFM coupling. The complete cancellation of magnetic moments, however, fails to arise owing to the different spin sites; hence, lead to a net magnetic moment. Weak ferromagnet which also known as canted AFM exhibits when incomplete cancellation of magnetic moments occur to the systems with equivalent and canted spin. All types of FM, AFM and ferrimagnetic ordering arise below a critical temperature, T_c. For FM ordering, the first discovery is on $[Fe(C_5Me_5)_2]^+$[TCNE = tetracyanoethylene) which orders below the T_c of 4.8 K [37]. While for FM ordering which rises from AFM coupling of the spins with different magnitude was first reported in 1984 by Alain Gleizes and Michael Verdaguer [38].

Magnetic materials have been in the center of interest since it provides major contributions to technological applications. For instance, it is widely used in the data storage industry including computer hard disks, credit cards, video recorders and many more. Magnetic materials also contribute to other aspects of our lives such as

in medical instrument and automobile. Technological applications formally use iron-based or rare earth materials. Such kind of materials leads to limitations for the magnetic materials applications. Organic magnet materials hence received considerable interest as an alternative to the silicon and metals due to the less effort of preparation in terms of time and money.

2.2 Mott Insulator

In 1973, Jan Hendrik de Boer and Evert Johannes Willem Verwey have revealed that transition metal oxides which are measured to be conductors by band theory are insulators. This is rationalized in terms of electron-electron interactions suggested by Nevill Mott and Rudolf Peierls which are neglected in band theory. For a better understanding of Mott-insulator, the effects of strong interactions of the electrons must take into account. Mott insulator will develop when the d shells are half-filled and both valance band and conduction band are composed of transition-metal d states. In addition, the occurrence of Mott insulator also depends on the repulsive Coulomb potential, U which should be sufficient to produce an energy gap. By tuning certain parameters such as magnetic field, pressure, voltage and composition, Mott insulator can turn into a conductor. This effect is widely known as a Mott transition. This kind of transition can be applied to invent applications like field-effect transistors, memory devices and switches [39].

Hubbard model can provide a deep understanding of how the system can occur in both metallic and insulating behavior. This model considers a lattice with one electron for each site. For two electrons located on the same site would take a Coulomb repulsion U due to their negative charge. In addition, transfer integral, t

presence between two neighboring sites. There are two quantities of physical characteristic for each system in this Hubbard model which are Coulomb repulsion U and bandwidth whilst the behavior of the system represented by the ratio, U/W. Conceptually, Mott transition is developed when $U/W = 1$.

The theoretical and experimental studies pertaining to this topic are continuously performed as it is still an open question. A double perovskite Ba_2NaOsO_6 (BNOO) is one of the compounds in this Mott insulator class. Through thermodynamic and reflectivity measurements previously, this material is identified to be 5d FM Mott insulator with an ordered moment of ~ 0.2 μ_B per formula unit [40]. Subsequently, μSR experiment has clarified the value of the ordered moment by previous measurements [41]. In 2015, the theoretical calculations by using hybrid DFT have been performed to determine BNOO compound. In this study, spin-orbit coupling (SOC) is included and consequently developed FM Mott insulating ground state. Hence, BNOO is considered as a Mott insulator at quarter filling, owing to the strong exchange-correlation and large SOC [42].

Despite the importance of Mott transition, critical behavior has remained controversial.

2.3 BEDT-TTF Molecule

Bis(ethylenedithio)tetrathiafulvalene abbreviated as BEDT-TTF or ET has been extensively studied until recently. On the contrary of other organic molecular metals which shows characteristics of one-dimensional (1D) array of the donors, BEDT-TTF molecule show two-dimensional (2D) characteristic indicated from the

investigation of the HOMO intermolecular overlap integrals resulting from the forming of conduction bands [43]. From the computational study by French *et al*., they have reported that the HOMO of the BEDT-TTF molecule is of carbon double bond (C = C) bonding and carbon – sulphur single bond (C – S) antibonding character [44]. In addition, the structures are stacked side-by-side instead of face-to-face stacking and the band structure is slightly different from other organic molecular metals. BEDT-TTF compound possesses the highest T_c among organic superconductors. In 1986, Kobayashi *et al.* have reported on the crystal structure of the neutral BEDT-TTF molecule [45]. From the experiment, this system is crystalized in a monoclinic symmetry with the space group of $P2_1/c$ and the values of *a*, *b* and *c* are 6.614, 13.985 and 16.646 Å, respectively. They have determined the mean bond length of C – S and C = C to be 1.751 Å and 1.327 Å, respectively. They also found that the C = C bonds become longer while C – S bonds become shorter with the increasing formal charge of BEDT-TTF molecule. This is happened due to the symmetry of HOMO of BEDT-TTF which contains nodal planes on each C – S bond. The ethylene of the 6-membered rings was found to be nonplanar which results in a staggered conformation with C_2 symmetry and an eclipsed conformation with C_s symmetry. It has previously been ascribed that the ethylene conformation can influence the structural and physical properties of the ET salts [14, 26]. The energy for both confirmations is almost the same. The side-by-side arrangement of this insulating neutral molecule shows an interesting characteristic as the feature is similar to the conducting BEDT-TTF. This compound will form ET, ET^+, or $(ET)_2^+$ when coupled with an acceptor.

2.4 $(BEDT\text{-}TTF)_2X$ Compound

BEDT-TTF compounds which are well-known with their strong electron correlation are formed by an organic cation (BEDT-TTF) and the inorganic anion part (X). These types of series exhibit a various characteristic feature such as insulating, metallic, superconducting and semiconducting phases as the molecular arrangement of the conducting part is varied. The ET part which is a conducting part plays the main role for constructing this layered organic material. The π orbitals of the sulphur atoms of adjacent molecules are close in contacts resulting in 2D molecular bands. The insulating part which alternates with the conducting part plays an important role in the charge transfer which results in partially filled molecular bands.

Owing to the specific steric effects, the strong side-by-side overlap between π-orbitals of adjacent molecules takes place [47]. The lower binding energy of the π-electrons results in the π-hole character of the free charge carrier. The two central carbon atoms in the cation part are nonequivalent due to the dimerization of ET molecules [48].

The different possible packing motifs of the ET molecules are designated by the Greek letters; *α, β, κ, δ, λ*, and so forth. The physical properties of the different packing motifs varied due to the changes in the molecular overlap and the transfer integrals. The typical characteristic is the layered crystal structure. In contrast to other polymorphic phases, where the donor molecules form stacking configuration, strong structural dimerization configured by two face-to-face ET molecules is formed in the *κ*-phase packing. Generally, *κ*-ET molecule has a quarter of hole for each HOMO band since it is a nature of charge transfer salt. The dimerization in the

structure, however, changes the filling of antibonding HOMO from quarter-filled to the half-filled band. Hence, each hole in the dimers is serving as carriers in the system. The charge carriers on the dimers lead to the formation of the triangular lattice.

κ-(BEDT-TTF)$_2$Cu[N(CN)$_2$]X (X=Cl, Br, and I) which also abbreviated as κ-ET is a part of charge-transfer salts materials. There are two ET layers in one unit cell, which are layer A and layer B. In one layer, they consist of two inequivalent ET dimers with ½ holes per dimer and various monovalent anions, X as can be seen in Figure 2.1 below. The conducting ET dimers are located on the corners and centers of a rectangular lattice [49]. The orientation between both dimers on the corners and centers are different with the angle nearly 90°. The dimers donate one of the electrons to the anion, hence leave one hole behind. The hole in the dimer results in a half-filled electronic band, which is very crucial for the requirement of the Mott-insulating state. On the other hand, the cross-section of the Fermi surface is equal to the first Brillouin zone.

The dimers which are located in the cation layer are arranged on an anisotropic triangular lattice and packed perpendicular to each other and form a checkerboard pattern. The dimers are stacking via π orbitals which situated on sulphur atoms. The donors are generated by the delocalization of corresponding π-electrons. They are dimerized in a head-to-tail configuration and related by centrosymmetry [50]. The cation layer lies in the ac-plane while the anion layer is a long polymeric chain extended along *a* direction. The anion part forms a closed shell and does not responsible for electronic conduction and magnetism.

Specifically, κ-ET molecules are inclined with respect to the conducting sheet by $\delta = 34°$. Instead of a square lattice, the lattice in the conducting plane is elongated along the *a*-axis due to this inclination [49].

Due to the simplicity of the electronic properties of this compound, it can provide knowledge on basic characteristics such as magnetism, superconductivity and electronic band formation by application of chemical and hydrostatic pressures.

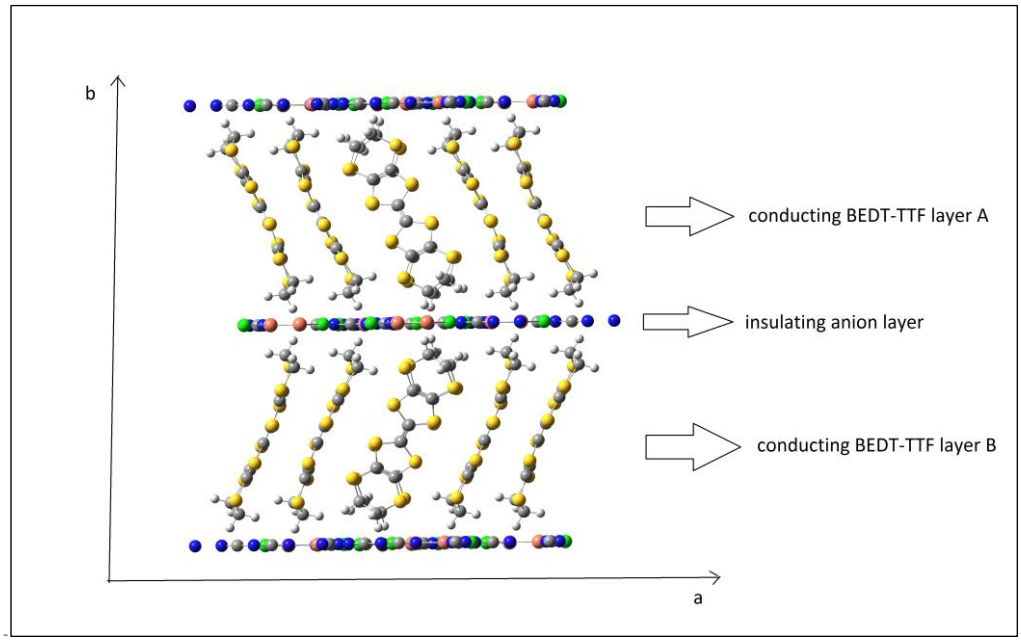

Figure 2.1 Crystal structure of κ-ET from *c*-axis direction

Charge-transfer salts are created when a donor molecule in a system has donated an electron to an acceptor molecule which is also known as an anion to form a compound. It is responsible to bind the charge-transfer salt together. The donor part of a charge-transfer salt is packing nearly so that the molecular orbitals overlap. The conformations of the donor part are responsible to determine the electronic properties of the system.

These kinds of materials have received much attention due to their great potential application in spintronic devices. Its properties which are tunable with respect to the lattice parameters also lead κ-ET as a very intriguing compound both to experimental and theoretical researchers. They exhibit a various type of behaviors including superconducting, magnetic ordering, Mott insulating and so forth when manipulating the external parameters such as chemical substitution, temperature, pressure and others due to the weak bonding energies. From the superconducting point of view, κ-type salts exhibit the highest T_c among ET's family. Their superconducting properties are proved to be different albeit there are in the same family. As κ-Br exhibit unconventional superconducting state at ambient pressure [14], κ-I did not show the superconducting state under any conditions, while κ-Cl is a paramagnetic insulator. It shows metallic properties and also exhibits superconducting properties at T_c= 11.5 K at ambient pressure [15]. The lattice arrangement that is the softness of the crystal lattice is responsible for the presence of the superconducting effect [15]. In κ-Cl and κ-Br, the ethylene end groups are believed to be ordered in an eclipsed arrangement at low temperatures. Hence, the absence of superconducting in κ-I is possibly due to the disorder of the lattice.

The substitution of atoms by different isotopes is another feasible tuning mechanism. It can be either partial or full replacement of hydrogen atoms in the ethylene groups of the ET dimers with deuterium atoms, which lead to the chemically-induced shift from metallic towards the Mott insulating state in both cases. For example, the measurement on deuterated κ-$(ET)_2Cu[N(CN)_2]Br$ previously have shown a non-uniform T_c shift [51]. The T_c shift was detected to be around 4 – 5 % larger than predicted by a simple mass change of the isotope-substituted materials. This difference can be explained in terms of the geometrical

isotope effect. In addition, the deuterated system exhibit higher sensitivity with the presence of the magnetic fields. From the dc magnetization experiment on hydrogenated and deuterated κ-Cl by Ito *et al.*, they have found that the magnetic phase diagram of the deuterated system shifts to higher temperature and pressure as compared to hydrogenated system. This result proved that the weak FM state is more stable for the deuterated system. The result, however, is in contrast with the κ-Br compound in which the superconducting state is more stable for the hydrogenated system [52]. One possible explanation is the fact that the larger unit cells of the deuterated system weaken the molecular interaction, therefore allow high degrees of freedom for spin ordering. In addition, the transfer integral and the dipole-dipole interaction of deuterated system is generally smaller than those of hydrogenated system [18].

κ-ET also has an interesting aspect in the magnetism, in which the AFM correlation are subject to the frustrated triangular lattice.

Spin liquid phases is another intriguing properties in κ-ET which depend on the temperature, pressure and the anion part. The series of κ-(BEDT-TTF)$_2$Cu[N(CN)$_2$]X is also a strongly correlated system which the interactions between the electrons give a major contribution on the electronic properties of the systems.

Recently, Watanabe *et al.* perform a theoretical study on ¾-filled extended Hubbard model by using a Monte Carlo method to investigate the various electronic phases in molecular conductors κ-(BEDT-TTF)$_2$Cu[N(CN)$_2$]X [10]. From the research, a few different phases were discovered; paramagnetic metal (PM), superconductor, dimer-Mott insulator with AF spin order, two charge-ordered

insulator and 3-fold charge-ordered metal. All the phases ultimately generated owing to the cooperation between the on-site and inter-site Coulomb.

The studies on these organic molecular materials are continuously performed since the nature of the superconducting state is still an open question. The Cooper pair pairing symmetry is one of the keen topics. Few experiments were performed to study the superconducting pairing including the ac susceptometer [53], muon spectroscopy resonance (μSR) [54], scanning tunnelling spectroscopy (STM) [55] and so forth. Some of the researchers support conventional *s* wave pairing while some others suggest unconventional pairing. The relation of superconductivity with the fundamental structural quantities remains unclear.

There are a few compounds of κ-BEDT-TTF that are well-studied in this class of materials such as κ-Cl and κ-Br. This thesis has focused on the κ-Cl and deuterated κ-Br compound as both of them exhibit AFM ordering.

2.5 κ-(BEDT-TTF)$_2$Cu[N(CN)$_2$]Cl

This Mott insulator compound has an orthorhombic crystal structure with a space group *Pnma* and Z=4 [15]. It consists of a cation layer which is BEDT-TTF (abbreviated as ET) molecule and insulating anion layer which is stacked alternately and lies in the ac plane. The anions that form inert are generally non-magnetic layers (Cu is in the Cu^{1+} state) which play an important role as a charge reservoir. The $(ET)_2^+$ layers are responsible for charge transport and magnetism. Due to the close packing of ET molecules, the electron orbits overlap is high. As a consequence, the charge can move freely within the layers and leads to a high interlayer conductivity. Based on band electronic structure calculations along with considerations of electron

count, κ-Cl is proposed to be a two-dimensional metal with a half-filled conduction band [56].

Numerous studies of κ-Cl have been reported including experimental and theoretical studies. It has attracted increasing attention among researchers as this compound possesses the complete sequence of states, namely, the Mott-insulating, AFM, metallic, and superconducting states, emerges by the pressure of a few hundred bars [36, 37, 38]. According to Schirber *et al.*, κ-Cl was shown to be superconducting under a very slight hydrostatic pressure, 0.3 kbar which consider as the lowest in an organic superconductor [60]. In other literature, Wang *et al.* have also proved that superconductivity exhibited at the same pressure with the highest reported superconducting transition temperature, 12.8 K [16]. Despite abundance results are reported in the literature, the origin and the estimated temperature of superconducting states are still subject to ongoing controversies.

Apart from superconducting properties exhibited by κ-Cl, it is also undergoes a phase transition into an AFM insulating state when the pressure is below the value of 0.3 kbar. This phase transition is widely known as the Mott-insulating transition. The presence of AFM ordering was proved by Welp *et al*. through magnetization measurement [61]. The transition was revealed near 45 K. They also suggested that this system is a Hubbard-Mott insulator. Experiments by Miyagawa *et al.* on a single crystal of $Cu[N(CN)_2]Cl$ using ^1H NMR for the first time and also magnetization measurement has shown a slight difference in the magnetic transition which the AFM ordering started to occur below 26 – 27 K with a moment of (0.4 – 1.0)μ_B/dimer [62]. The magnetic moment determined by Smith *et al.* is 0.5μ_B/dimer, which is in a good agreement with the results obtained by Miyagawa *et al.*[63]. In another piece of literature, the magnetic moment obtained is slightly different from

Smith *et al.*, which is 0.45μ_B/dimer [64]. The differences can be rationalized in terms of variation of spectroscopies utilized in the studies.

According to Kawamoto *et al.*, the origin of the AF transition is a strong electrons correlation instead of nesting of open Fermi surfaces [65]. This conclusion is made based on the characteristic of the AF states which is contradicted from the conventional spin-density wave (SDW). The insulator-to-metal transition also can be understood as a Mott transition driven by a strong electron correlation, instead of the nesting of the Fermi surface [66].

In addition, weak FM hysteresis near 22 K with a moment of (8×10-4)μ_B/formula was discovered for the first time in this class of materials [61]. While, the results by Miyagawa *et al.* revealed that the weak ferromagnetism starts to occur below 23 K due to spin canting. The canting, however, is very small and the spins are nearly antiparallel with an easy axis perpendicular to the layers. An easy axis was interpreted to be along the *b*-axis owing to the presence of a spin-flop transition at approximately 0.3 T. The result on the easy axis by Miyagawa *et al.*, subsequently was verified by Pinterić *et al.* [67]. The experiment from the same author has also reported on the canted AFM spins exhibited below 22 K by an angle of 6×10^{-2} degrees from *b*-axis. On the contrary, further experiment on the easy axis using antiferromagnetic resonance (AFMR) has reported the different result [68]. They have discovered easy-plane anisotropy with an easy plane at around 35º from the *a*-*c* plane. Due to Smith *et al.* by the magnetization measurement, the transition of weak ferromagnetism from AFM is likely driven by Dzyaloshinsky-Moriya (DM) interaction [63]. They have proposed to include exchange term, a DM term, an anisotropic exchange term, and a Zeeman term in the model that explains the observed electron spin ordering. The DM term is taking into consideration for the

canting which it is responsible for the orientation of the spins in the plane perpendicular to the external field. According to Smith *et al.,* the DM vector must be perpendicular to *c* plane. They have also proposed that the interplane DM interaction is weaker than the intraplane DM interaction, since the exchange coupling is weaker in between the planes.

By using NMR and ESR measurements, Antal *et al.* however, has proposed that the DM vectors, are oriented differently in A and B layers which lie in the (*a*,*b*) plane at φ_A = 46.5° and φ_B = 133.5°, renders the DM vector of two adjacent layers are nearly perpendicular to each other [69]. The discovery of DM interaction by Smith *et al.* are in agreement with the conclusion by Pinterić *et al*. in which, they have suggested that a large hysteresis of the spin flop transition along with FM moment can be attributed to DM interaction [67].

In 2008, Kagawa *et al.* have performed magnetization and NMR measurement for better understanding of κ-Cl magnetism [70]. From both experiments, they have observed that the application of a uniform field induces a staggered moment perpendicular to the applied field. From the experimental and numerical results obtained, they inferred that the field-induced staggered moment in the paramagnetic phase also arises from the contribution of DM interactions. The experiments discussed above mostly were carried out under an external magnetic field. The external magnetic field, however, can be problematic owing to the fact that it can break spatial-continuous symmetry.

On that account, μSR techniques under zero-field environment can be an extremely useful method to overcome the limitations due to its high sensitivity of the magnetic ordering. This kind of experiment has using a positive muon as a local

probe to investigate the properties of the system. Muon can be a very good probe since their mass is very light which is $1/9^{th}$ the mass of a proton. Recently, Ito *et al.* have performed μSR experiment on zero-field magnetism of κ-Cl [20]. The study has proposed five possible sites for muon to attach. They also observed two distinct muon spin precession and one relaxation signal. The values of the internal fields at the muon sites are 58.4 ± 0.4 G and 42.9 ± 0.3 G. They proposed five muon stopping sites that are A, B, C, D and E with the magnitudes of the internal fields generated by the single dimer of 58 G, 68 G, 58 G, 74 G and 18 G respectively. The values of internal fields at A, B, C and D sites are comparable to the observation. They also performed low-field magnetization measurements and reported the value of T_N as 22.80 $\pm$ 0.02 K.

Apart from the unique characteristic in magnetism, κ-Cl also possesses intriguing properties such as multiferroicity. In 2012, P. Lunkenheimer *et al.* have discovered a new behavior of κ-Cl that is multiferroicity which observed the ordering of electrical and magnetic properties concurrently [71]. The ferroelectric behavior exhibited below 27 K, which in accord with crossover onset temperature. In another literature, Pinterić *et al*. have also identified the magnetic and dielectric properties that disclose the formation of two mutually uncorrelated magnetic subsystems which can be related to the donor and acceptor, respectively [67].

In addition to the experimental studies, the underlying anisotropic triangular lattice of this system also was theoretically investigated by Kandpal *et al.* by utilizing band structure calculation [72]. The results obtained show that κ-Cl and other three derivatives are less frustrated as compared to the data obtained previously via semi-empirical theory [73]. This conclusion can be quantitatively explained in terms of t'/t ratios which yield smaller values and hence indicate a lower frustration. In other

literature, electronic and geometrical structures of this compound are investigated by Imamura *et al.* using *ab initio* MO methods [74]. They have calculated the ionization potential, transfer integrals, Coulomb interactions, Fermi surface and band dispersion. The long-range Coulomb interaction was calculated by a 2-D extended Hubbard model. They have discovered that the intradimer Coulomb interaction, V_{int}, enhances the dimer on-site Coulomb interaction, which controls the paramagnetic metal and AF state transition. In 2002, Kawakami *et al.* have performed UHF and UDFT methods to calculate the effective exchange integral, $J_{ab(M)}$ and $J_{ab(D)}$ [75]. The values of $J_{ab(D)}$ obtained for molecules 1, 2 and 3 are -71.6, -71.6 and -30.2 respectively. From the calculations, they have concluded that the spin-lattice of BEDT-TTF compound including κ-Cl is a square planar which is in contrast with the previous calculation that assumed the spin-lattice to be triangular. Subsequently, the theoretical study from the same author has confirmed that 2D interaction is dominant for κ-phase of BEDT-TTF [76].

From all the experimental and theoretical studies performed, electron correlation is inferred to play an important role to produce a wide variety of electronic phases and also act as a driving force of the metal-insulator transition in κ-ET.

The wide diversity and unique properties owned by κ-Cl render them as a suitable compound to produce selected devices such as spintronic devices. They also have applications in thin-film magnetic heterostructures and high-temperature superconductivity. In addition, κ-Cl is very useful to invent the smaller field-effect transistor, memory devices and switches.

Despite an abundance of experiments were carried out on this compound, the electronic properties in the vicinity of the Mott-insulating state are still an open question. The data accumulated from experiments conducted under pressure also remained scattered and restricted by the selectivity of the experimental spectroscopy used.

2.6 *κ*-d8-(BEDT-TTF)$_2$Cu[N(CN)$_2$]Br

Particular attention has been devoted to *κ*-d8-(BEDT-TTF)$_2$Cu[N(CN)$_2$]Br since the phase transition lies in the vicinity of a first-order line in the phase diagram [17]. A deuterated compound of *κ*-BEDT-TTF)$_2$Cu[N(CN)$_2$]Br will form when all the hydrogens in this system are replaced by deuterium atoms. A deuterium atom is one of the stable isotopes of hydrogen. Substitution of hydrogen by deuterium atom does not affect the electronic structure of the system since both hydrogen and deuterium contain one proton at each nucleus. It only differs in the number of a neutron. The chemical properties are also nearly identical since it depends on the atom's electronic configuration which relates to a number of protons. The X-ray diffraction measurement on *κ*-Br by Komatsu *et al*. also have proved that the unit cell parameters obtained are similar between hydrogenated and deuterated systems [77]. The results imply that the substitutions of the isotope are isostructural with the original system in which the conducting sheets are formed by donor molecules in the *ac* plane. The difference between hydrogen and deuterium however, can be explained in terms of the (negative) chemical pressure emerged from the small difference between C – H and C – D bond lengths [78]. The difference of the bonds ultimately depends on the different behaviors of the H – and D – bonds owing to the large